ENVIRONMENTAL RESEARCH
LETTERS

LETTER • OPEN ACCESS

Improved modelling of soil NO_x emissions in a high temperature agricultural region: role of background emissions on NO_2 trend over the US

ENVIRONMENTAL RESEARCH
LETTERS

LETTER

Improved modelling of soil NO_x emissions in a high temperature agricultural region: role of background emissions on NO_2 trend over the US

Yi Wang[1,2,*], **Cui Ge**[1,2,3], **Lorena Castro Garcia**[1,2], **G Darrel Jenerette**[4], **Patty Y Oikawa**[5] **and Jun Wang**[1,2,*]

[1] Center for Global and Regional Environmental Research, Iowa Technology Institute, The University of Iowa, Iowa City, IA 52242, United States of America
[2] Department of Chemical and Biochemical Engineering, The University of Iowa, Iowa City, IA 52242, United States of America
[3] South Coast Air Quality Management District, Diamond Bar, CA 91765, United States of America
[4] Department of Botany and Plant Sciences, University of California, Riverside, CA 92521, United States of America
[5] Department of Earth and Environmental Sciences, California State University, East Bay, Hayward, CA 94542, United States of America
* Authors to whom any correspondence should be addressed.

E-mail: jun-wang-1@uiowa.edu **and** yi-wang-4@uiowa.edu

Keywords: soil NO_x emissions, OMI NO_2, high temperature, trend

Supplementary material for this article is available online

OPEN ACCESS

RECEIVED
16 February 2021

REVISED
19 July 2021

ACCEPTED FOR PUBLICATION
21 July 2021

PUBLISHED
6 August 2021

Abstract

EPA reports a steady decline of US anthropogenic NO_x emissions in 2005–2019 summers, while NO_2 vertical column densities (VCDs) from the OMI satellite over large spatial domains have flattened since 2009. To better understand the contributing factors to a flattening of the OMI NO_2 trends, we investigate the role of soil and lightning NO_x emissions on this apparent disagreement. We improve soil NO_x emissions estimates using a new observation-based temperature response, which increases the linear correlation coefficient between GEOS-Chem simulated and OMI NO_2 VCDs by 0.05–0.2 over the Central US. Multivariate trend analysis reveals that soil and lightning NO_x combined emissions trends change from $-3.95\%\ a^{-1}$ during 2005–2009 to $0.60\%\ a^{-1}$ from 2009 to 2019, thereby rendering the abrupt slowdown of total NO_x emissions reduction. Non-linear inter-annual variations explain 6.6% of the variance of total NO_x emissions. As background emissions become relatively larger with uncertain inter-annual variations, the NO_2 VCDs alone at the national scale, especially in the regions with vast rural areas, will be insufficient to discern the trend of anthropogenic emissions.

1. Introduction

NO_x ($NO + NO_2$) emitted mainly from anthropogenic sources, wild fires, lightning, and soil plays a significant role in catalysing tropospheric ozone production and destruction and forming nitrate aerosols (Schindlbacher *et al* 2004, Seinfeld and Pandis 2016). National Emissions Inventory (NEI) reports a steady decrease of anthropogenic NO_x emissions during 2005–2019 summers at a mean rate of $-4.12\%\ a^{-1}$ over the contiguous US. Ozone Monitoring Instrument (OMI) tropospheric vertical column densities (VCDs), however, show a consistent decline until 2009, and a flattened trend afterwards up to 2015 (Jiang *et al* 2018). Silvern *et al* (2019) shows that the inconsistence between NEI and VCD trends during 2009–2017 reflect the variation of background emissions (soil and lightning sources). To date, the impact of soil NO_x emissions on the observational NO_2 trends remains quantitively elusive.

Soil NO_x emissions are an important source during summer (Vinken *et al* 2014, Huber *et al* 2020), and their strength is mainly influenced by fertilizer application, soil moisture, and soil temperature. Unusually high soil NO_x emissions are observed over high-temperature agricultural regions in California where fertilized soil is a major source of NO_x pollution (Oikawa *et al* 2015, Almaraz *et al* 2018). Moreover, nearly half of the enhancement of O_3 production that is related to rising temperature over the southeast US can be caused by the rising soil NO_x emissions due to the increase of soil temperature (Romer *et al* 2018).

Here, we use satellite observations and a chemistry transport model (CTM) to improve estimates of soil NO_x emissions, and subsequently, to quantify the impact of soil NO_x on the slowdown of observed NO_2 VCD reduction and examine the sources for inter-annual variation of total NO_x emissions beyond the trend analysis. In various CTMs, soil NO_x emission estimates are often parameterized as a function of biome types, soil moisture and temperature, N-pulsing, N-deposition, and fertilizer maps (Yienger and Levy 1995, Steinkamp and Lawrence 2011, Hudman *et al* 2012, Rasool *et al* 2016, 2019). Two of uncertainties are the dependence of soil NO_x emissions on soil temperatures especially in high temperature conditions and the simplification for soil temperature estimations. Notably, the emissions response to soil temperature in these CTMs is assumed to be flat after soil temperature is above 30 °C. Berkeley-Dalhousie Soil NO_x Parameterization (BDSNP) is the state-of-the-art scheme, which is implemented in GEOS-Chem, a widely used CTM; we will improve it using a new observation-based relationship between soil surface NO_x flux and soil temperature from Oikawa *et al* (2015) over the US in high temperature (above 30 °C) conditions. Furthermore, in existing GEOS-Chem, soil temperature as a key input variable to BDSNP is derived from 2 m air temperature through linear and empirical relationships that vary only with soil and canopy types (Yienger and Levy 1995). Hence, the soil temperature in the Modern-Era Retrospective analysis for Research and Applications, Version 2 (MERRA-2) dataset is used here directly to further refine BDSNP, thereby collectively formulating a new scheme, hereafter BDISNP, in which 'I' stands for Iowa.

Finally, the inconsistency between the trends of satellite-observed NO_2 and anthropogenic NO_x emissions is investigated. With the improved soil emissions scheme, we quantitively attribute the slowdown of satellite-observed NO_2 decreasing trend to different sectors and suggest that it is partly due to the co-variations of natural emissions and the trends thereafter among different sectors (such as soil and lightning).

2. GEOS-Chem modelling

2.1. BDISNP scheme with new function for high temperature

GEOS-Chem is a 3D chemistry transport model that is driven by meteorological re-analysis fields (GEOS-FP or MERRA-2). In its BDSNP scheme (Hudman *et al* 2012, Vinken *et al* 2014), the soil temperature response is identical to the exponential function ($f(T) = e^{0.103T}$) for wet soil in YL95 (Yienger and Levy 1995) for temperature between 0 °C and 30 °C, and is constant once soil temperature is above 30 °C (blue line, figure 1). This study replace the old temperature function with a new observation-based temperature function (orange line, figure 1) from Oikawa *et al* (2015), and the rest parameterizations are unchanged. In the range of 20 °C–40 °C, it is a cubic function of soil temperature ($f(T) = -0.009T^3 + 0.837T^2 - 22.527T + 196.149$). The value of the cubic function is close to the YL95 function in the range of 20 °C–23 °C, and it becomes larger than the exponential function as soil temperature increases from 23 °C to 40 °C. The cubic function is a factor of 1.4 and 2.7 larger than the exponential function at 30 °C and 40 °C, respectively. When soil temperature is above 40 °C, temperature function is set as the value of the cubic function at 40 °C. The YL95 exponential function is now used for soil temperature between 0 °C and 20 °C.

2.2. Experimental design

We use version 12.7.2 GEOS-Chem driven by MERRA-2 meteorological fields to simulate soil NO_x emissions and atmospheric NO_2 concentrations over the US, with a spatial resolution of 0.5° × 0.625° and 47 vertical layers from surface to stratopause in summer (June, July and August) during 2005–2019. The boundary conditions required by the nested simulations are provided by global 2° × 2.5° simulations (Wang *et al* 2004). Anthropogenic emissions are distributed using the NEI2011 inventory scaling to different years according to national annual totals (EPA 2021). Open fire emissions are from the fourth-generation Global Fire Emission Database (GFED4) daily emission inventory (Giglio *et al* 2013). Lightning NO_x emissions are calculated using the lightning flash densities and convective-cloud depths that are derived from the MERRA-2 data and distributed following the monthly redistribution factors generated using the Lightning Imaging Sensor and Optical Transient Detector (LIS/OTS) high resolution monthly climatology (Murray *et al* 2012).

Three sensitivity experiments with different treatments of soil NO_x emissions are used to explore the impacts of the updated scheme (BDISNP) on soil NO_x emissions and atmospheric NO_2 concentrations. The Control and T_{new} runs use BDSNP and BDISNP, respectively, while soil NO_x emissions are turned off in the NO_SOIL experiment. Following Silvern *et al* (2019), the soil NO_x emissions are reduced by 50% for the control and T_{new} runs, based on the previous comparison between GEOS-Chem simulations and OMI NO_2 VCDs showing the overestimation of soil NO_x emissions using BDSNP (Vinken *et al* 2014).

3. OMI and surface NO_2 and GEOS-Chem data processing

Tropospheric NO_2 VCDs from the version 4.0 NASA OMI NO_2 L2 standard product (OMINO2) (Lamsal *et al* 2021) at a spatial resolution of 13 × 24 km^2

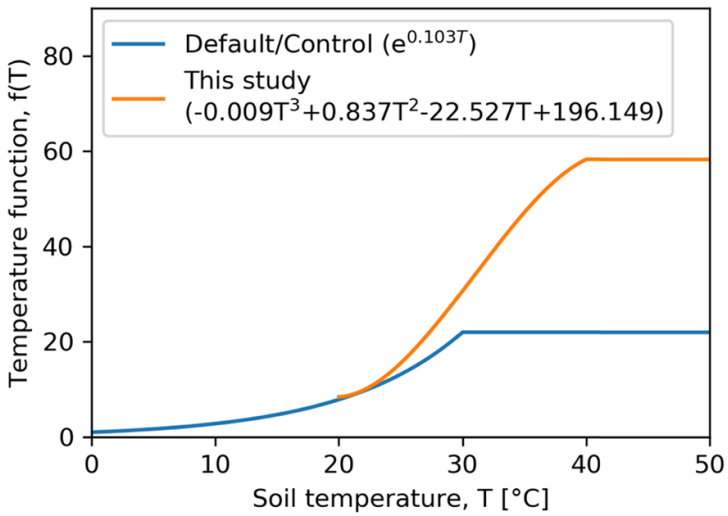

Figure 1. Default (blue line) and revised observation-based (orange line, this study) temperature-dependent soil NO_x emissions functions in GEOS-Chem. Note, the two functions only differ at temperature above 20 °C.

at nadir are used to evaluate the GEOS-Chem simulations. The product has a swath of 2600 km and an equator-crossing time at 13:45, hence providing contiguous global coverage daily (Levelt *et al* 2006). Retrievals are error prone to large Solar Zenith Angles (SZA) and large View Zenith Angles (VZA), high cloud contamination, and snow cover; thus only data with SZA < 75°, VZA < 65°, effective cloud fraction < 0.3, terrain reflectivity < 0.3 are used (Wang *et al* 2020a). Moreover, the pixels that are affected by row anomaly (Schenkeveld *et al* 2017) or not flagged as high quality are removed.

In situ surface NO_2 measurements during 2005–2019 are available at EPA Air Quality System (AQS), and most of these observational sites are located in urban regions. Despite of systematic positive bias due to the measuring method (Steinbacher *et al* 2007), the measurement are still useful for model evaluations (Wang *et al* 2020b).

For proper comparison, GEOS-Chem NO_2 simulations are sampled according to OMI observing time and converted to the tropospheric VCDs using the scattering weights, tropospheric air mass factors (AMFs), and tropopause pressure from the OMINO2 product (Wang *et al* 2020a). Comparison of GEOS-Chem surface NO_2 with surface *in situ* data from EPA is spatially and temporally paired, following the method in Wang *et al* (2020b).

4. Approaches for trend analysis

A statistical framework with treatment of covariance of emissions in each sector is conceived for the trend analysis and attribution, and to quantitively link the linear trend and inter-annual non-linear variation of NO_x emissions from these sectors to the variance of total NO_x emissions, hence explaining the atmospheric NO_2 trend observed by satellite. Firstly, total NO_x emissions consist of the trend parts and inter-annual variability parts of each sectors shown as:

$$E_i^{\mathrm{t}} = \sum_{j=1}^{N} E_{i,j}^{\mathrm{tr}} + \sum_{j=1}^{N} E_{i,j}^{\mathrm{vr}} = \sum_{j=1}^{N} c_j + \sum_{j=1}^{N} b_j \cdot i + \sum_{j=1}^{N} E_{i,j}^{\mathrm{vr}} \tag{1}$$

where E represents NO_x emissions, t, tr, and vr are short for total, trend, inter-annual variability, respectively, i and j are indexes of year and sector, respectively, N is total number of sectors including anthropogenic, soil, lightning, and fires, c and b are intercept and slope (trend) of E^{tr}, respectively, which are derived through linear regression.

Following past studies, the relative trends of total ($b^{\mathrm{rel,t}}$) and sectoral (b_j^{rel}) NO_x emissions since 2005 are the focus of this study; their relationship is shown as:

$$\begin{aligned} b^{\mathrm{t}} &= \sum_{j=1}^{N} b_j \\ \left(b^{\mathrm{t}} \div E_{2005}^{\mathrm{t}}\right) \cdot E_{2005}^{\mathrm{t}} &= \sum_{j=1}^{N} \left(b_j \div E_{2005,j}\right) \cdot E_{2005,j} \\ b^{\mathrm{rel,t}} \cdot E_{2005}^{\mathrm{t}} &= \sum_{j=1}^{N} b_j^{\mathrm{rel}} \cdot E_{2005,j} \\ b^{\mathrm{rel,t}} &= \sum_{j=1}^{N} b_j^{\mathrm{rel}} \cdot \frac{E_{2005,j}}{E_{2005}^{\mathrm{t}}} \end{aligned} \tag{2}$$

Furthermore, we show that the variance of total NO_x emission can be divided into: (a) the covariances between sectoral trend parts and total NO_x emissions and, (b) the covariances between

sectoral inter-annual variability parts and total NO_x emissions:

$$\begin{aligned}\mathrm{Var}\left(\boldsymbol{E}^{\mathrm{t}}\right) &= \mathrm{Var}\left(\sum_{j=1}^{N}\boldsymbol{E}_j\right) = \mathrm{Var}\left(\sum_{j=1}^{N}\boldsymbol{E}_j^{\mathrm{tr}} + \sum_{j=1}^{N}\boldsymbol{E}_j^{\mathrm{vr}}\right)\\ &= \mathrm{Cov}\left(\boldsymbol{E}^{\mathrm{t}}, \sum_{j=1}^{N}\boldsymbol{E}_j^{\mathrm{tr}}\right) + \mathrm{Cov}\left(\boldsymbol{E}^{\mathrm{t}}, \sum_{j=1}^{N}\boldsymbol{E}_j^{\mathrm{vr}}\right)\\ &= \sum_{j=1}^{N}\mathrm{Cov}\left(\boldsymbol{E}_j^{\mathrm{tr}}, \boldsymbol{E}^{\mathrm{t}}\right) + \sum_{j=1}^{N}\mathrm{Cov}\left(\boldsymbol{E}_j^{\mathrm{vr}}, \boldsymbol{E}^{\mathrm{t}}\right)\end{aligned} \tag{3}$$

where Var and Cov represent variance and covariance operator, respectively, $\boldsymbol{E}$ is a data vector consisting time series of the NO_x emissions data. Hence, the contribution of sectoral linear trend to the variance of total NO_x emissions can be computed as $\mathrm{Cov}\left(\boldsymbol{E}_j^{\mathrm{tr}}, \boldsymbol{E}^{\mathrm{t}}\right)/\mathrm{Var}\left(\boldsymbol{E}^{\mathrm{t}}\right)$, while $\mathrm{Cov}\left(\boldsymbol{E}_j^{\mathrm{vr}}, \boldsymbol{E}^{\mathrm{t}}\right)/\mathrm{Var}\left(\boldsymbol{E}^{\mathrm{t}}\right)$ is the part of total emission variance explained by the non-linear sectoral inter-annual variability. Subsequently, the trend part of the variance of total NO_x emissions, $\mathrm{Var}\left(\boldsymbol{E}^{\mathrm{tr,t}}\right)$, is essentially the sum of covariances between sectoral emission trend ($\boldsymbol{E}_j^{\mathrm{tr}}$) and total emission trend ($\boldsymbol{E}^{\mathrm{tr,t}}$):

$$\begin{aligned}\mathrm{Var}\left(\boldsymbol{E}^{\mathrm{tr,t}}\right) &= \mathrm{Var}\left(\sum_{j=1}^{N}\boldsymbol{E}_j^{\mathrm{tr}}\right) = \mathrm{Cov}\left(\boldsymbol{E}^{\mathrm{tr,t}}, \sum_{j=1}^{N}\boldsymbol{E}_j^{\mathrm{tr}}\right)\\ &= \sum_{j=1}^{N}\mathrm{Cov}\left(\boldsymbol{E}_j^{\mathrm{tr}}, \boldsymbol{E}^{\mathrm{tr,t}}\right)\end{aligned} \tag{4}$$

Hence, for each sector j, its contribution to the linear trend of total emissions can be computed as $\mathrm{Cov}\left(\boldsymbol{E}_j^{\mathrm{tr}}, \boldsymbol{E}^{\mathrm{tr,t}}\right)/\mathrm{Var}\left(\boldsymbol{E}^{\mathrm{tr,t}}\right)$.

5. Results

5.1. Evaluation of BDISNP

T_{new} produces soil NO_x emissions of 201 Gg N summer^{-1} over the US, which is 18.2% higher than that from Control. Moreover, during the hot days when daily mean soil temperatures are greater than 30 °C, T_{new} has 32.6% more soil NO_x emissions than Control. Large soil NO_x emissions from Control (figure 2(a)) are mainly over Central US and California, where agricultural activity is intense. Compared with Control, T_{new} simulates the increase of soil NO_x emissions up to 120% mainly in south of 40°N (figure 2(c)) where soil temperature is high and consequently, the new temperature response function is important. In north of 40°N, up to 47% decrease of soil NO_x emissions exists (figure 2(c)), which is caused by that MERRA-2 soil temperature (T_{new}) is lower than that calculated from 2 m temperature using linear and empirical approach (Control) in these regions.

Evaluation of GEOS-Chem simulations with OMI tropospheric VCDs mainly focuses on temporal linear correlation coefficients between them, which are highly relevant to the linear trend analysis. Compared with the Control run (figure 3(a)), T_{new} shows the increase of linear correlation coefficient (R) in the range of ∼0.05 to ∼0.2 over the Central US (black box in figure 3(b)), where fertilizer activities are intense and soil NO_x emissions play a significant role. The small decrease (usually less than 0.04) of R is also found over the North Dakota, northern Minnesota, and central Texas. Overall, BDISNP improves on BDSNP in terms of R values over the US when evaluating with OMI tropospheric NO_2 VCDs.

The improvement of R over the Central US is caused by the better simulations of tropospheric NO_2 VCDs over high soil temperature conditions (>30 °C). Figure 3(c) show the changes of tropospheric NO_2 VCDs from OMI and the GEOS-Chem simulations as soil temperature increases over the Central US. When soil temperature is less than 30 °C, the difference between Control and T_{new} is negligible (results not shown). In the soil temperature range of 30 °C to 40 °C, the tropospheric NO_2 VCD from T_{new} is larger than Control, and the difference increases as soil temperature rises (figure 3(c)). T_{new} has larger positive bias than the Control (figure 3(c)), but the positive bias is not caused by the parameterization for emissions dependence on temperature; even if soil NO_x emissions are excluded in the GEOS-Chem simulation (NO_SOIL), modeled NO_2 VCD is still larger than OMI observation (figure 3(c)). The positive bias likely originates from the overestimation of other terms in NO_x emission schemes (that this study does not revise) or other error sources in GEOS-Chem. Furthermore, the uncertainties from NO_2 slant column fitting, tropospheric-stratospheric separation (with year to year variability and is most relevant for rural studies), and air mass factor calculation (Bucsela *et al* 2013) all contribute to the uncertainty of OMI tropospheric NO_2 VCD, which is estimated as 35% (Lamsal *et al* 2021), and all the bias in T_{new} is within the uncertainty envelope (shaded area in figure 3(c)) of OMI observational error (Lamsal *et al* 2021). We assume that NO_2 VCD difference between OMI and the GEOS-Chem simulations are independent of soil temperature, correcting the GEOS-Chem systematic bias by subtracting the difference for all conditions with soil temperature above 30 °C. With this non-temperature dependent bias correction (figure 3(c)), T_{new} well captures the increase of OMI tropospheric NO_2 VCD observations as a function of soil temperature, while both Control and NO_SOIL underestimate the characteristics (figure 3(d)); the Normalized Centered Root Mean Square Error (NCRMSE) (Wang *et al* 2020a) is 0.089 for T_{new}, which is much smaller than 0.266 and 0.421 for Control and NO_SOIL, respectively (figure 3(d)). As to the decrease of

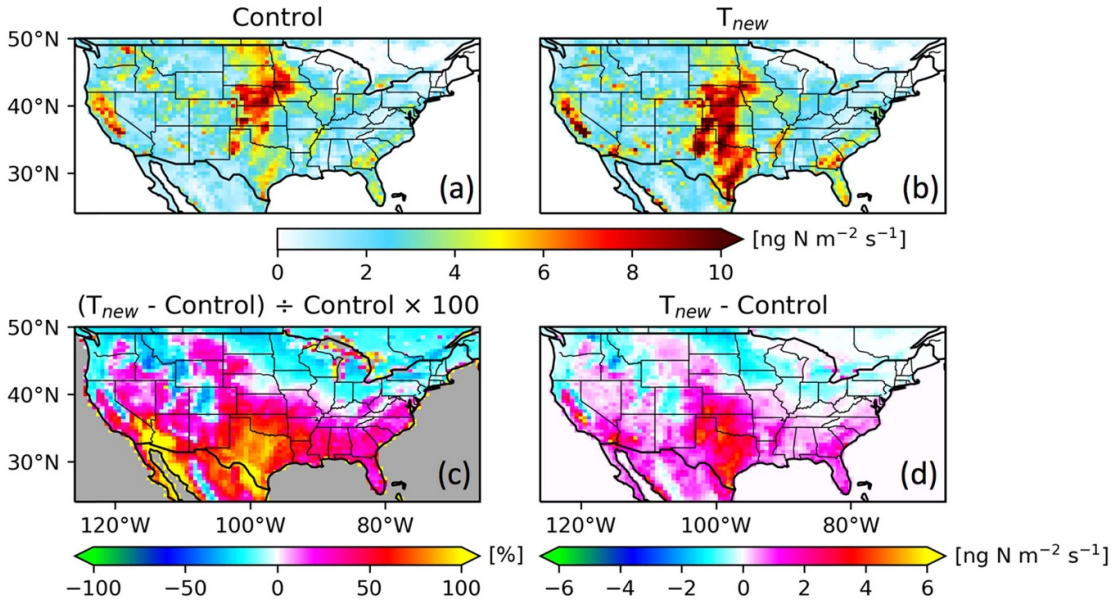

Figure 2. Soil NO_x emissions during 2005–2019 summers from Control (a), T_{new} (b), their relative difference (c), and difference (d).

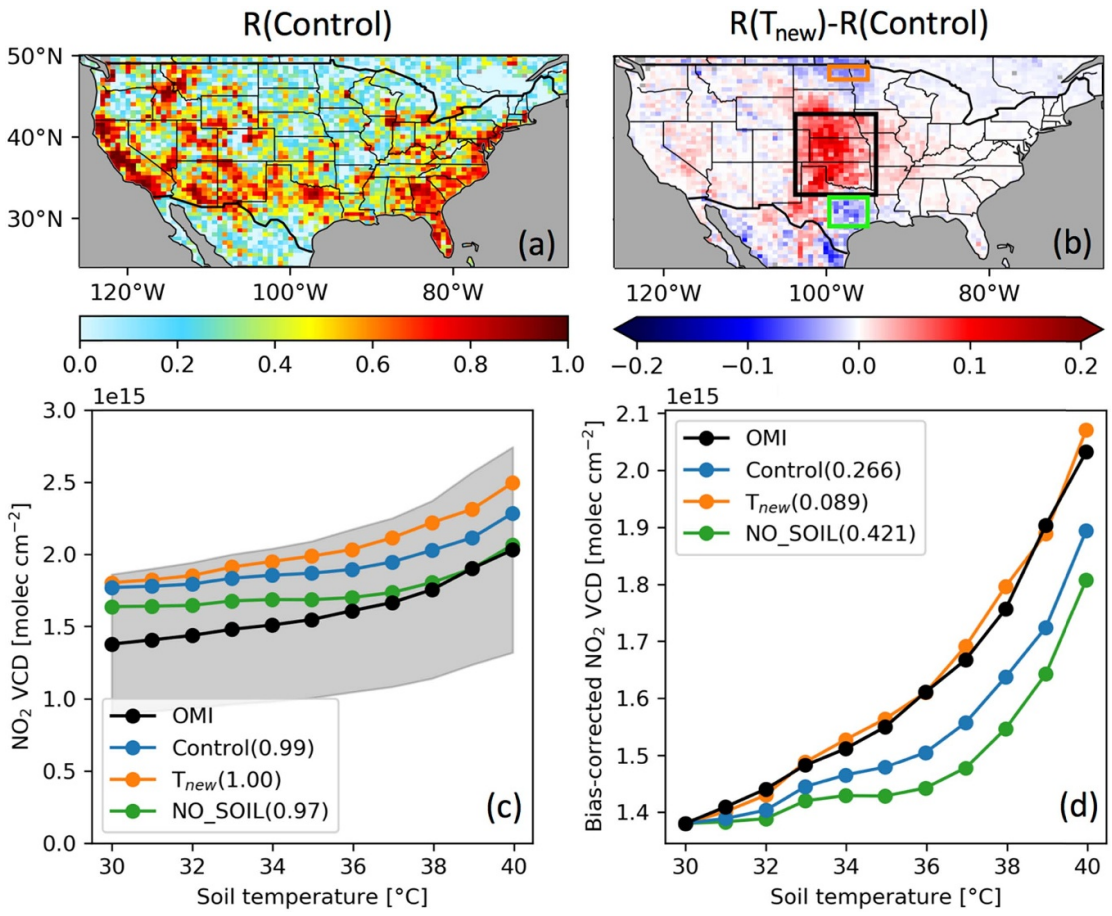

Figure 3. The map of the linear correlation coefficients (R) between OMI and Control tropospheric NO_2 VCDs (OMI-control) (a), and the difference of R values between OMI-T_{new} and OMI-Control (b) is during 2005–2019 summers. (c) Shows the changes of tropospheric NO_2 VCDs from OMI (black), Control (blue), T_{new} (orange), and NO_SOIL (green) as a function of soil temperature over the Central US (black box in (b)). Each point represents the average of tropospheric NO_2 VCDs for the OMI overpass time soil temperatures between 30 °C and 40 °C at an interval of 2 °C. Shaded area in grey denotes the envelope of uncertainty of OMI tropospheric NO_2 VCD. Numbers in the legend of (c) are linear correlation coefficients. (d) Is similar to (c) except that the results from GEOS-Chem simulation are subtracted by their corresponding biases at soil temperature of 30 °C in reference to the OMI VCD. Numbers in the legend of (d) are normalized centered root mean square error.

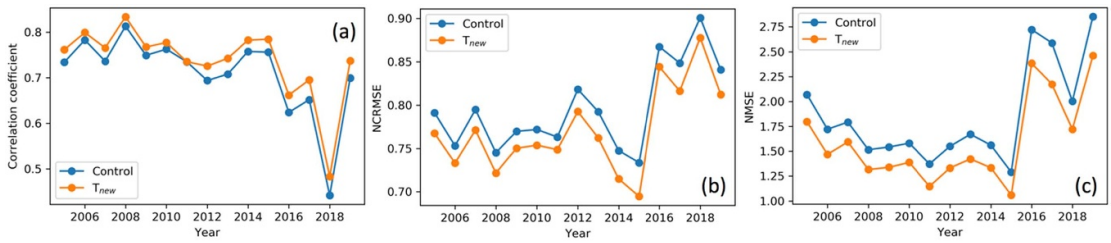

Figure 4. Evaluation of surface NO_2 concentrations from the Control (blue) and T_{new} (orange) runs with EPA *in situ* observations in term of linear correlation coefficient (a), normalized centered root mean square (NCRMSE) (b), and Normalized Mean Square Error (NMSE) (c). Only sites where the ratio of soil to total NO_x emissions is greater than 0.2 are used for evaluation.

R over North Dakota/Minnesota (orange box in figure 3(b)) and Texas (green box in figure 3(b)), figure S1 (available online at stacks.iop.org/ERL/16/084061/mmedia) shows that OMI NO_2 VCDs are almost constant in temperature ranges of 20 °C–30 °C and 30 °C–38 °C for North Dakota/Minnesota and Texas, respectively, while all GOES-Chem simulations (Control, T_{new}, and NO_SOIL) show NO_2 VCDs increase as soil temperature rises. As GEOS-Chem cannot properly simulate NO_2 VCDs in the two regions, the new scheme even renders a decrease of R.

GEOS-Chem surface NO_2 concentrations from Control and T_{new} are also evaluated with EPA *in situ* observations. Surface NO_x concentrations between T_{new} and EPA have R values ∼0.02–0.03 larger than of that from the Control almost each summer (figure 4(a)), while NCRMSE and normalized mean square error (NMSE) decrease in the range of 2.0%–5.3% (figure 4(b)) and 11.1%–17.9% (figure 4(c)), respectively, each summer.

5.2. Quantifying background contributions to NO_x variations

Figures 5(a) and (b) show the relative trends (b^{rel}) since 2005 of NO_x emissions from T_{new} and tropospheric NO_2 VCDs from OMI and the GEOS-Chem simulations in contagious US, respectively. Total NO_x emissions show a steady decline during 2005–2019, primarily reflecting the trend of its dominant source—the anthropogenic NO_x emissions (figure 5(a)). Starting from 2009, however, the decline trend of total NO_x emissions becomes less than half of that during 2005–2009 (figure 5(a)). OMI tropospheric NO_2 VCDs observe a steady decline from 2005 to 2009 and a flattening afterward, supporting the existence of the turning point of total NO_x trend in 2009 as simulated by T_{new} (figure 5(b)), and the stronger slowdown of NO_2 VCDs reduction in Central US than in Western and Eastern US implies that NO_x emissions from natural sources contribute to the slowdown (figure S2). Therefore, the fidelity of T_{new} in simulating the NO_x VCD variation (section 5.1 and figure 5(b)) enables further quantitative attribution of relative trend of total NO_x emissions to role of emissions from each sector.

The relative trend since 2005 of total NO_x emissions is −2.75% a^{-1} (figure 5(a)); it equals the sum of the relative trends of every sector weighted by the ratio of sectoral to total NO_x emissions in 2005 (equation (2)). NO_x emissions from fires sector have the largest positive relative trend of 6.49% a^{-1} (figure 5(a)), but its contribution to the relative trend of total NO_x emissions is negligible, as the percentage of fires sector to total NO_x emissions is only 0.87% in 2005 and 1.89% during 2005–2019. The contributions of soil, lightning, and anthropogenic sector to total NO_x emissions in 2005 are 11.15%, 16.10%, and 71.88%, respectively. Hence the relative trend of total NO_x emissions is mainly affected by these three sources. The relative trend of anthropogenic NO_x emissions is −4.12% a^{-1}, while soil sector has a weaker downward trend of −1.44% a^{-1} and lightning sector has an upward trend of 1.94% a^{-1} (figure 5(a)). As a result, despite the large steady decrease of NO_x emissions from anthropogenic source, total NO_x emissions trend is weakened by the impacts of the increase of lightning emissions and the weaker decrease of soil emissions to reach −2.75% a^{-1} overall during 2005–2019.

The trends relative to 2005 in the periods of 2005–2009 and 2009–2019 for different NO_x emissions sources are calculated (table 1) to investigate the abrupt slowdown of total NO_x emissions reduction starting in 2009. The relative decreasing trend in total NO_x emissions is −5.19% from 2005 to 2009, which is 120% stronger than that during 2009–2019. The relative trend in anthropogenic NO_x emissions is only 53% stronger during 2005–2009 than that from 2009 to 2019. The much larger slowdown of the total NO_x emissions reduction than that of anthropogenic source is caused by the difference between the two periods for relative trends in soil and lightning NO_x emissions. The relative trends in lightning and soil sources during 2005–2009 are −1.15% a^{-1} and −8.00% a^{-1}, respectively, and their weighted mean is −3.95% a^{-1}; by contrast, their combination shows an upward relative trend of 0.60% a^{-1} from 2009 to 2019. The change of the directions of the relative trends largely contribute to the slowdown of total NO_x emissions reduction. The temporal variation of

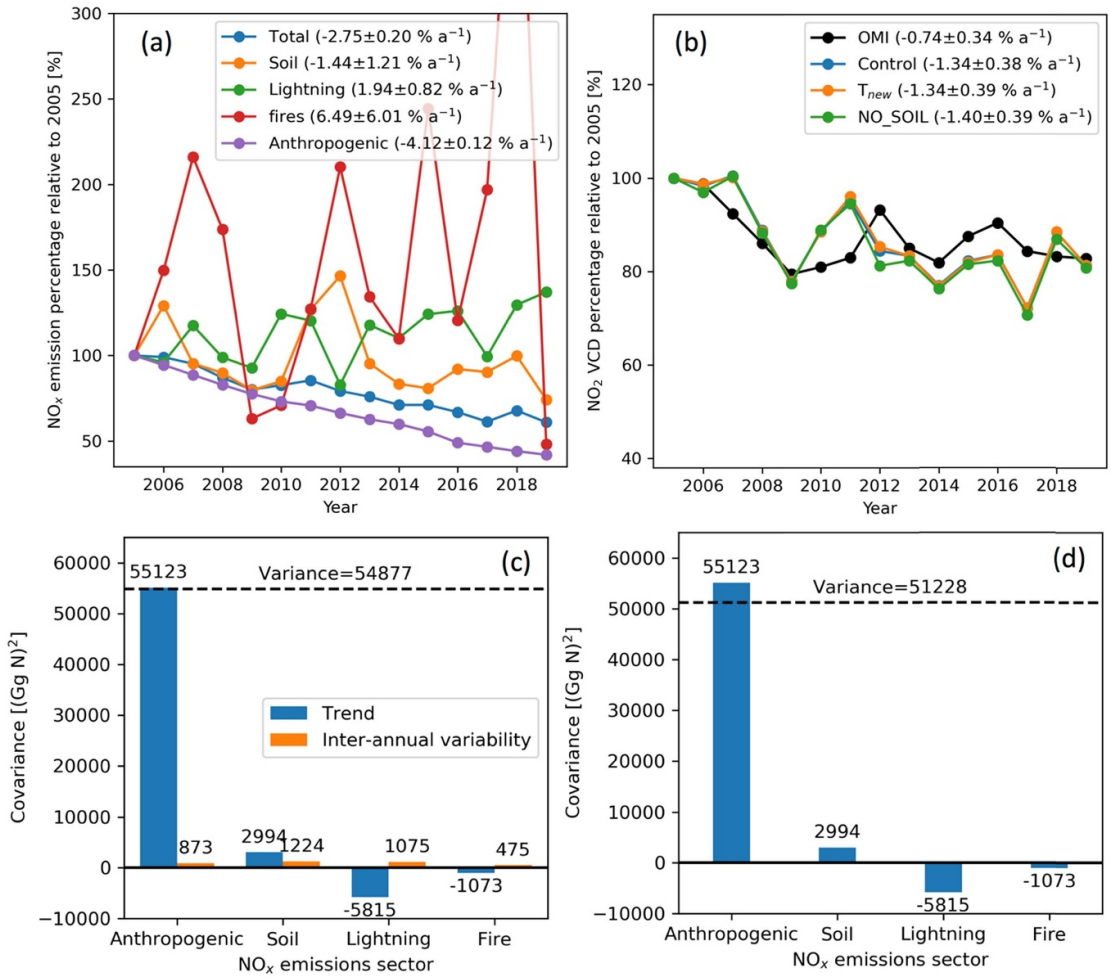

Figure 5. Relative trends since 2005 of (a) NO_x emissions by sectors from T_{new}, (b) tropospheric NO_2 VCDs derived from OMI and the GEOS-Chem Control, T_{new}, and NO_SOIL simulations in contiguous US. (c) Is the decomposition of the variance of total NO_x emissions (black dash line) according to equation (3) with each bar showing the covariance of component and total NO_x emissions. (d) Is the decomposition of the variance of the trend in total NO_x emissions (black dash line) according to equation (4) with each bar showing the covariance of component trend and trend in total NO_x emissions.

Table 1. The NO_x emissions trends relative to the start year of various time periods for difference sources (units: % a^{-1}).

	2005–2019	2005–2009	2009–2019
Total	−2.75 ± 0.20	−5.19 ± 0.84	−2.34 ± 0.32
Anthropogenic	−4.12 ± 0.12	−5.66 ± 0.05	−3.71 ± 0.11
Lightning	1.94 ± 0.82	−1.15 ± 3.44	2.48 ± 1.47
Soil	−1.44 ± 1.21	−8.00 ± 4.96	−1.82 ± 2.11
Fires	6.49 ± 6.01	−5.01 ± 21.82	14.74 ± 10.66

soil NO_x emissions are mainly affected by soil temperature and soil moisture rather than the change of fertilizer (S1 in supplement).

In addition to linear trends, we investigate the contribution of sectoral emissions to the inter-annual non-linear variations of NO_x emissions following equation (3). The covariance between anthropogenic trend part and total NO_x emissions is 55 123 (Gg N)^2 (gigagram N squared), which is slightly larger than the variance of total NO_x emissions of 54 877 (Gg N)^2 (figure 5(c)). The sum of covariances between sectoral trends and total NO_x emissions is 51 229 (Gg N)^2, suggesting that the linear trend among each sector can explain 93.4% of the variance of total NO_x emissions, while the non-linear inter-annual variability explain 6.6% (figure 5(c)). Similarly, following equation (4), we find that the contribution of anthropogenic, soil, lightning, and fire sources to the trend of total NO_x emissions in terms of variance are 107.60%, 5.84%, −11.35%, and 2.09%, respectively, in contagious US, and these values are 103.9%, 11.6%, −15.8%, 0.2% in Central US (defined

in figure S2(a)). Thus, the non-linear inter-annual variability also plays an important role, and its contribution is expected to increase as anthropogenic NO_x emissions decrease over time.

6. Discussion and conclusions

We revised Berkeley-Dalhousie Soil NO_x Parameterization (BDSNP) in GEOS-Chem by (a) allowing the increase of soil NO_x emission with temperature up to 40 °C (instead of 30 °C in BDSNP) based on *in situ* observations, and (b) using the soil temperature directly from MERRA-2 (instead of indirectly deriving soil temperature from air temperate as in implemented in standard GEOS-Chem), hence forming the new BDSINP (where 'I' stands for Iowa) scheme. Compared to the GEOS-Chem simulation with BDSNP, using BDSINP overall yields better agreement with OMI NO_2 climatology; the linear correlation coefficients between simulated and OMI-observed tropospheric NO_2 VCDs during 2005–2019 summer increase by 0.05–0.2 over the Central US, where soil NO_x emissions dominate. Furthermore, GEOS-Chem with BDSINP renders a tropospheric NO_2 VCDs response function to temperature that is more consistent with the counterpart independently derived from a combined analysis from OMI and MERRA-2 data.

With its improved fidelity, GEOS-Chem simulation with BDSINP is used to disentangle the covariance among different NO_x emission sectors toward understanding the slowdown of tropospheric NO_2 VCD reduction during 2009–2019. A statistical framework is proposed to decompose the variance of total NO_x emission into linear and non-linear parts, and further offer a quantitative approach to attribute each part to the linear and non-linear variation of emissions from each sector. GEOS-Chem simulation with BDSINP is able to capture the linear trend of OMI tropospheric NO_2 VCDs, both showing a decreasing trend during 2005–2009 summer and a level-off after 2009. Indeed, in the total variance of total NO_x emissions in 2005–2019, ~93.4% can be explained by linear trends from each sector, in which anthropogenic, soil, lightning, and fire sources contribute 107.60%, 5.84%, −11.35%, and 2.09%, respectively; the negative contribution of lightning emissions means they are negatively correlated with total NO_x emissions, hence dampening the trend in total NO_x emissions. The remaining 6.6% is due to non-linear inter-annual variations of each sector and their co-variations among each sector, and such non-linear inter-annual variations is expected to increase in the next decade as anthropogenic emissions continue to decline while natural variations due to fires, lightning, and soil are expected to increase. Due to the impact of soil and lightning emissions on the total trend and the contribution of non-linear inter-annual variations to the variation of total NO_x emissions, a linear trend derived from the satellite observations in rural areas would be difficult to discern the trend of anthropogenic emissions.

This study has quantified that NO_x natural sources (soil and lightning) contribute to the slowdown of NO_2 VCDs reduction, although the roles of anthropogenic source and atmospheric chemistry could be important and should be investigated in the future research. We have simulated the slowdown of NO_2 VCDs reduction starting at 2009 with the input of the EPA's emission inventory that presented the steady (and more or less linear) reduction of anthropogenic NO_x emissions. In the past studies, Jiang *et al* (2018) reported another inventory that showed the slowdown of the reduction of anthropogenic NO_x emissions due to 'the growing relative contribution of industrial, area, and off-road mobile sources of emissions, decreasing relative contribution of on-road gasoline vehicles, and slower than expected decreases in on-road diesel NO_x emissions', and used it to explain the slowdown of the reduction of atmospheric NO_2; in contrast, Silvern *et al* (2019) showed that both trends of two inventories from EPA and Jiang *et al* (2018) are within the uncertainty of AQS surface NO_2 trends. Therefore, which anthropogenic inventory is more realistic is still open to discussion. However, this study showed quantitively the importance of soil and lightning NO_x in explaining the slowdown starting at 2009 (other than in the years prior to or after 2009), and pointed out that the linear trend only partially explains the variance of atmospheric NO_2 with time. While chemistry and anthropogenic emissions both play a role in the slowdown (as pointed by Laughner and Cohen (2019) and Jiang *et al* (2018)), this study reveals that the importance of soil emissions should not be overlooked toward a better understanding of the slowdown of atmospheric NO_2 reduction, especially over the Central US where the slowdown is more significant than Eastern or Western U.S. (figure S2). An improved soil NO_x emission scheme for the Central U.S., as developed in this study, can be used to further detangle the relative role of chemistry, anthropogenic emissions, and natural source emissions in the change of atmospheric NO_2 with time.

Data availability statement

The data that support the findings of this study are openly available at the following URL/DOI: https://disc.gsfc.nasa.gov/datasets/OMNO2_003/summary?keywords=omi%20no2 (OMI NO_2 product), https://aqs.epa.gov/aqsweb/airdata/download_files.html (EPA *in situ* NO_2), http://wiki.seas.harvard.edu/geos-chem/index.php/GEOS-Chem_12#12.2.0 (GEOS-Chem source code and all required emission inventories (including GFED4 and NEI2011) other inputs), www.epa.gov/air-emissions-inventories/air-pollutant-emissions-trends-data

(EPA national annual anthropogenic NOx emissions totals).

Acknowledgments

This work was supported by NASA Atmospheric Modeling and Analysis program (Grant Nos. NNX17AF77G and 80NSSC19K095), National Science Foundation (Grant No. DEB-1656062), USDA (Award No. 2019-67021-29227), and NOAA (Award No. NA19OAR4310178).

ORCID iD

Jun Wang https://orcid.org/0000-0002-7334-0490

References

Almaraz M, Bai E, Wang C, Trousdell J, Conley S, Faloona I and Houlton B Z 2018 Extrapolation of point measurements and fertilizer-only emission factors cannot capture statewide soil NO_x emissions *Sci. Adv.* **4** eaau7373

Bucsela E J, Krotkov N A, Celarier E A, Lamsal L N, Swartz W H, Bhartia P K, Boersma K F, Veefkind J P, Gleason J F and Pickering K E 2013 A new stratospheric and tropospheric NO_2 retrieval algorithm for nadir-viewing satellite instruments: applications to OMI *Atmos. Meas. Tech.* **6** 2607–26

EPA 2021 *Annual Average Emissions, Air Pollutant Emission Trends Data* (available at: www.epa.gov/air-emissions-inventories/air-pollutant-emissions-trends-data) (Accessed 28 January 2021)

Giglio L, Randerson J T and Van der Werf G R 2013 Analysis of daily, monthly, and annual burned area using the fourth-generation global fire emissions database (GFED4) *J. Geophys. Res.* **118** 317–28

Huber D E, Steiner A L and Kort E A 2020 Daily cropland soil NO_x emissions identified by TROPOMI and SMAP *Geophys. Res. Lett.* **47** e2020GL089949

Hudman R, Moore N, Mebust A, Martin R, Russell A, Valin L and Cohen R 2012 Steps towards a mechanistic model of global soil nitric oxide emissions: implementation and space based-constraints *Atmos. Chem. Phys.* **12** 7779–95

Jiang Z *et al* 2018 Unexpected slowdown of US pollutant emission reduction in the past decade *Proc. Nat. Acad. Sci.* **115** 5099–104

Lamsal L N *et al* 2021 Ozone Monitoring Instrument (OMI) Aura nitrogen dioxide standard product version 4.0 with improved surface and cloud treatments *Atmos. Meas. Tech.* **14** 455–79

Laughner J L and Cohen R C 2019 Direct observation of changing NO_x lifetime in North American cities *Science* **366** 723–7

Levelt P F, Oord G H J V D, Dobber M R, Malkki A, Huib V, Johan De V, Stammes P, Lundell J O V and Saari H 2006 The ozone monitoring instrument *IEEE Trans. Geosci. Remote Sens.* **44** 1093–101

Murray L T, Jacob D J, Logan J A, Hudman R C and Koshak W J 2012 Optimized regional and interannual variability of lightning in a global chemical transport model constrained by LIS/OTD satellite data *J.Geophys. Res.* **117** D20307

Oikawa P, Ge C, Wang J, Eberwein J, Liang L, Allsman L, Grantz D A and Jenerette G D 2015 Unusually high soil nitrogen oxide emissions influence air quality in a high-temperature agricultural region *Nat. Commun.* **6**

Rasool Q Z, Bash J O and Cohan D S 2019 Mechanistic representation of soil nitrogen emissions in the Community Multiscale Air Quality (CMAQ) model v 5.1 *Geosci. Model Dev.* **12** 849–78

Rasool Q Z, Zhang R, Lash B, Cohan D S, Cooter E J, Bash J O and Lamsal L N 2016 Enhanced representation of soil NO emissions in the Community Multiscale Air Quality (CMAQ) model version 5.0.2 *Geosci. Model Dev.* **9** 3177–97

Romer P S *et al* 2018 Effects of temperature-dependent NO_x emissions on continental ozone production *Atmos. Chem. Phys.* **18** 2601–14

Schenkeveld V M E, Jaross G, Marchenko S, Haffner D, Kleipool Q L, Rozemeijer N C, Veefkind J P and Levelt P F 2017 In-flight performance of the ozone monitoring instrument *Atmos. Meas. Tech.* **10** 1957–86

Schindlbacher A, Zechmeister-Boltenstern S and Butterbach-Bahl K 2004 Effects of soil moisture and temperature on NO, NO_2, and N_2O emissions from European forest soils *J.Geophys. Res.* **109** D17302

Seinfeld J H and Pandis S N 2016 *Atmospheric Chemistry and Physics: From Air Pollution to Climate Change* (New York: Wiley)

Silvern R F *et al* 2019 Using satellite observations of tropospheric NO_2 columns to infer long-term trends in US NO_x emissions: the importance of accounting for the free tropospheric NO_2 background *Atmos. Chem. Phys.* **19** 8863–78

Steinbacher M, Zellweger C, Schwarzenbach B, Bugmann S, Buchmann B, Ordóñez C, Prevot A S H and Hueglin C 2007 Nitrogen oxide measurements at rural sites in Switzerland: bias of conventional measurement techniques *J.Geophys. Res.* **112** D11307

Steinkamp J and Lawrence M G 2011 Improvement and evaluation of simulated global biogenic soil NO emissions in an AC-GCM *Atmos. Chem. Phys.* **11** 6063–82

Vinken G, Boersma K, Maasakkers J, Adon M and Martin R 2014 Worldwide biogenic soil NO_x emissions inferred from OMI NO_2 observations *Atmos. Chem. Phys.* **14** 10363–81

Wang Y X, McElroy M B, Jacob D J and Yantosca R M 2004 A nested grid formulation for chemical transport over Asia: applications to CO *J.Geophys. Res.* **109** D22307

Wang Y, Wang J, Xu X, Henze D K, Qu Z and Yang K 2020a Inverse modeling of SO_2 and NO_x emissions over China using multisensor satellite data—part 1: formulation and sensitivity analysis *Atmos. Chem. Phys.* **20** 6631–50

Wang Y, Wang J, Zhou M, Henze D K, Ge C and Wang W 2020b Inverse modeling of SO_2 and NO_x emissions over China using multisensor satellite data—part 2: downscaling techniques for air quality analysis and forecasts *Atmos. Chem. Phys.* **20** 6651–70

Yienger J and Levy H 1995 Empirical model of global soil-biogenic NO_x emissions *J.Geophys. Res.* **100** 11447–64